Journal of Biomolecular NMR, **14:** 209–221, 1999.
KLUWER/ESCOM

Hybrid-hybrid matrix structural refinement of a DNA three-way junction from 3D NOESY-NOESY

Varatharasa Thiviyanathan[a], Bruce A. Luxon[a], Neocles B. Leontis[b], Nishantha Illangasekare[a], David G. Donne[a] & David G. Gorenstein[a,*]
[a]*Sealy Center for Structural Biology & Department of Human Biological Chemistry & Genetics, University of Texas Medical Branch, Galveston, TX 77555-1157, U.S.A.;* [b]*Department of Chemistry, Bowling Green State University, Bowling Green, OH 43403-0213, U.S.A.*

Received 18 November 1998; Accepted 19 April 1999

Key words: MORASS, NOESY-NOESY, relaxation matrix analysis, three-way junction

Abstract

Homonuclear 3D NOESY-NOESY has shown great promise for the structural refinement of large biomolecules. A computationally efficient hybrid-hybrid relaxation matrix refinement methodology, using 3D NOESY-NOESY data, was used to refine the structure of a DNA three-way junction having two unpaired bases at the branch point of the junction. The NMR data and the relaxation matrix refinement confirm that the DNA three-way junction exists in a folded conformation with two of the helical stems stacked upon each other. The third unstacked stem extends away from the junction, forming an acute angle (∼60°) with the stacked stems. The two unpaired bases are stacked upon each other and are exposed to the solvent. Helical parameters for the bases in all three strands show slight deviations from typical values expected for right-handed B-form DNA. Inter-nucleotide imino-imino NOEs between the bases at the branch point of the junction show that the junction region is well defined. The helical stems show mobility (± 20°) indicating dynamic processes around the junction region. The unstacked helical stem adjacent to the unpaired bases shows greater mobility compared to the other two stems. The results from this study indicate that the 3D hybrid-hybrid matrix MORASS refinement methodology, by combining the spectral dispersion of 3D NOESY-NOESY and the computational efficiency of 2D refinement programs, provides an accurate and robust means for structure determination of large biomolecules. Our results also indicate that the 3D MORASS method gives higher quality structures compared to the 2D complete relaxation matrix refinement method.

Abbreviations: CM, center of mass; FRET, fluorescence resonance energy transfer; MD, molecular dynamics; MORASS, multiple Overhauser relaxation analysis and simulation; PME, particle mesh Ewald; 3WJ, three-way junction.

Introduction

Considerable interest has arisen in the past to understand the structure of DNA three-way junctions (3WJ) as reviewed by Altona et al. (1996). DNA junctions play important roles as intermediates in genetic rearrangement processes such as recombination, transposition and integration events (Jensh and Kemper, 1986). 3WJs are observed as intermediates during the genetic recombination of phage DNAs and exist as structural elements in the terminal repeats of certain viruses. Adeno-associated virus (AAV), a DNA single strand virus that has a 3WJ in the terminal repeat regions (Bernks and Bohenzky, 1987), is emerging as a promising vector for virally mediated gene therapy (Anderson et al., 1997; Belague et al., 1997). 3WJs may also play a role in slipped-strand (s-DNA) structures of triplet repeat chromosomal DNA

*To whom correspondence should be addressed. E-mail: david@nmr.utmb.edu

which plays a role in over 12 human genetic diseases such as mytonic dystrophy, fragile X syndrome and Friedriech's ataxia (Chastain and Sinden, 1998). 3WJ structures occur frequently in functional RNA molecules. The hammerhead ribozyme (reviewed by Birikh et al. (1997) is a notable example of a catalytic RNA that is built around a 3WJ.

A variety of biophysical and biochemical techniques have been used to probe the structure of DNA 3WJs. 3WJs without any unpaired bases appear to be conformationally flexible, according to studies employing native gel electrophoresis (Duckett and Lilley, 1990; Zhong et al., 1994), chemical and enzymatic probing (Guo et al., 1990; Nussbaum et al., 1994), directed ligation (Ma et al., 1986; Shlyakhtenko et al., 1994), and FERT analysis (Stuhmeier et al., 1997a). 3WJs without unpaired bases in the junction region adopt an extended structure in which coaxial stacking of the helical arms is not possible without disruption of one of the basepairs. Naturally occurring 3WJs, however, invariably contain unpaired nucleotides at the branch point of the junction. Using native gel electrophoresis and optically monitored thermal denaturing experiments, it was shown earlier that the unpaired nucleotides in the junction region in fact stabilize the formation of DNA 3WJs (Leontis et al., 1991). The thermodynamics of formation of DNA 3WJs with (Ladbury et al., 1994) and without (Zhong et al., 1997) unpaired nucleotides has been studied by high-sensitivity isothermal titration calorimetry. Several NMR studies have been reported on the DNA 3WJ containing unpaired nucleotides (Leontis et al., 1993,1995; Rosen and Patel, 1993a,b; Overmars et al., 1996). Gel electrophoretic mobility shift experiments of DNA 3WJs show that in the presence of divalent metal ions, insertion of unpaired bases allows 3WJs to fold to form asymmetric structures where coaxial stacking exists between two helical stems (Welch et al., 1995). The folded structure appears to be most stable when the single-stranded bulge contains two or three bases. Recently reported FRET studies indicate that the overall geometry and conformational flexibility of the 3WJs are sensitive to the presence of unpaired bases (Yang and Miller, 1996; Stuhmeier et al., 1997a,b). The time resolved FRET studies also showed that the effects of bulges on the geometry and flexibility of 3WJs depend upon the type of the unpaired bases.

The structure determination of large biomolecules by high-resolution NMR methods can be limited by severe overlap of signals in 2D NOESY. Spectral overlap often prevents adequate measurement of sufficient NOEs from the 2D spectra, severely limiting the precision and accuracy of any refined structure. Spreading the spectral dispersion into a third, or even a fourth dimension is one way to overcome spectral over-crowding. For example, heteronuclear 3D NMR spectroscopy has been used to make the sequential assignments and obtain distance estimates. Homonuclear 3D NOESY-NOESY methods have been found to contain more information than 2D NOESY for quantitatively determining structures (Bonvin et al., 1991; Bernstein et al., 1993). Homonuclear 3D NOESY-NOESY has shown promise for structural determination of large biomolecules, since the dipolar cross-relaxation becomes more efficient with increasing molecular weight (Berg et al., 1990). Though the 3D NOESY-NOESY has a lower S/N ratio compared to the 2D NOESY, for large biomolecules where spectral overlap is a serious problem, 3D NOESY-NOESY holds the promise of providing more accurate structures, given the increased number of resolvable 3D NOESY-NOESY volumes. At high field and larger sample volumes, it may well be possible to obtain thousands of NOESY volumes.

Various methods have been developed for quantitative use of 3D NOESY-NOESY cross-peak intensities for structural refinements utilizing a two-spin approximation (Kessler et al., 1991), Taylor series expansion of the NOE-rate equation (Habazettl et al., 1992a,b), direct gradient refinement (Yip and Case, 1989; Bonvin et al., 1991), and hybrid-hybrid matrix (Zhang et al., 1995; Zhu et al., 1996). At realistic mixing times ($>$100 ms) that allow reasonably accurate measurement of 3D NOESY-NOESY volumes, both two-spin and the Taylor series expansion approximation methods can lead to considerable systematic errors (Donne et al., 1995). Direct structure refinement methods using 3D NOESY-NOESY spectra have been described to translate 3D peak intensities into distance restraints which are then used in restrained molecular dynamics (MD) calculations (Kessler et al., 1991), and to use 3D NOESY-NOESY peak volumes directly (Bonvin et al., 1991), instead of distance restraints, in structure refinement. Although the direct gradient method provides an accurate and precise means for structural refinement of 3D NOESY-NOESY data, it scales to the sixth power of the number of spins. An approximation to the gradient method was proposed that scales with the cube of the number of spins (Yip, 1993); however, in large systems this will still be computationally intensive. The deconvolution method proposed earlier

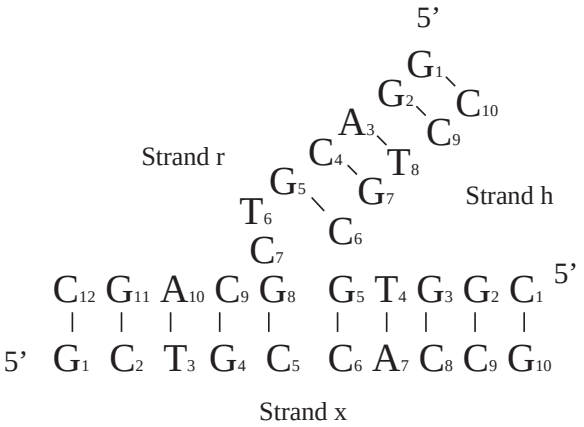

Figure 1. The sequence of the DNA 3WJ molecule used in this study. The 3WJ is composed of three DNA strands and has two unpaired pyrimidine bases in the junction region. The numbering of the strands and residues is based on the recommendation by an expert panel for the International Union of Biochemistry and Biophysics (Lilley et al., 1994). The strands are named as x, h, and r, and the helical arms are named as X, H, and R. For the numbering of residues, the strands are identified first followed by the bases. For example, x-G1 stands for the first guanine residue on strand x.

by our laboratory (Zhang et al., 1995) translated the 3D cross-peak intensities into 2D NOESY intensities, which can then be used to derive accurate distance restraints that can be used in structure refinement by an iterative relaxation matrix/ MD approach (Bothner-By and Noggle, 1979; Macura and Ernst, 1980; Keepers and James, 1984; Boelens et al., 1989a,b; Post et al., 1990; Lai et al., 1993). This hybrid-hybrid matrix approach avoids systematic errors while retaining computational efficiency. In simulation studies reported earlier, this methodology has proven to be effective, and validates the theory (Zhu et al., 1996).

In this paper, we demonstrate for the first time the capability of the hybrid-hybrid relaxation matrix method to experimentally refine the structure of a biomolecule, a DNA 3WJ containing 32 nucleotides (Figure 1). This paper also describes, for the first time, the application of restrained MD to study the conformational flexibility and dynamics of the three helical arms forming the 3WJ. This molecule has previously been investigated by 2D NMR spectroscopy (Leontis et al., 1995; Ouporov and Leontis, 1995).

Theory

In the two-spin approximation the volume of a 3D NOESY-NOESY cross peak between spins i, j and k is considered to be proportional to the product of the inverse sixth power of the distance between spins i and j and the distance between j and k,

$$A_{ijk}(\tau_{m1}, \tau_{m2},) \propto r_{ij}^{-6}(\tau_{m1}) \cdot r_{jk}^{-6}(\tau_{m2}) \qquad (1)$$

where $A_{ijk}(\tau_{m1}, \tau_{m2})$ is the 3D NOESY-NOESY volume, τ_{m1} and τ_{m2} are the two mixing periods, and r_{ij} is the inter-proton distance between spins a and b (Boelens et al., 1989a,b). While this approach provides a simple interpretation of the 3D NOESY-NOESY interaction, it does not include the effect of spin diffusion (due to multiple relaxation pathways) and therefore leads to dramatic systematic errors at realistic mixing times for larger biomolecules. A more complete analysis utilizes a complete relaxation matrix solution. The rate equation, without approximations, takes into account the cross relaxation between all spin pairs across the entire system and has the following form for a 3D NOESY-NOESY experiment:

$$A_{ijk}(\tau_{m1}, \tau_{m2}) = \exp(-\tau_{m2} R)_{kj} \cdot \exp(\tau_{m1} R)_{ij} A_i(0) \qquad (2)$$

where R is the rate matrix that describes the cross relaxation (σ_{ij}) and intrinsic longitudinal relaxation rates (ρ_i), and A(0) is the initial magnetization. The σ_{ij} is assumed to follow an isotropic tumbling model with a single correlation time, τ_c (determined by optimizing the match between theoretical and experimental NOEs).

Equation 2 may be written as:

$$A_{ijk}^{3D} \propto A_{ij}^{2D} \cdot A_{jk}^{2D} \qquad (3)$$

where A_{ij}^{2D} is the 2D NOESY volume between spins i and j. This equation can be rearranged such that a 2D volume can be calculated from the A_{ijk}^{3D} 3D volume:

$$A_{ij}^{2D} \propto A_{ijk}^{3D} / A_{jk}^{2D} \qquad (4)$$

The problem, of course, is obtaining values for the divisors. If the divisor volume is available experimentally, then it is taken from experiment. In the limits of larger molecular size, there will not be many resolved 2D peaks, which is the reason the 3D experiment is being performed. One solution is to obtain needed divisors from calculated data based on a model structure and the complete relaxation matrix solution to the Bloch equation,

$$A_{ij}^{2D} = \exp(-\tau_{m2} R)_{ij} A_i(0) \qquad (5)$$

In simulating the divisors, the first step is to simulate a hybrid 3D volume matrix allowing scaling of the 3D experimental and theoretical volumes and calculation of the 2D scaling volumes. However, only volumes needed for the deconvolution and a set of scaling volumes are simulated. The scaling set is actually the same set as those measured experimentally, with respect to the spin indices. The scaling factor S uses a linear regression:

$$S = \frac{\sum_{i=1}^{n}\sum_{j=1}^{n}\sum_{k=1}^{n} A_{ijk}^{theor}}{\sum_{i=1}^{n}\sum_{j=1}^{n}\sum_{k=1}^{n} A_{ijk}^{exp}} \quad (6)$$

where the summation is taken over all experimental 3D volumes. Since the model structure changes in each iteration, this scaling factor has to be re-evaluated at each iteration. Once the divisors have been scaled, the 3D experimental data is deconvoluted by Equation 4. If there is any available 2D NOESY experimental data, it is also scaled and included with the deconvoluted 2D data and any volume matrix elements not obtained from the experimental 3D or 2D spectra are calculated from the structure to yield a complete hybrid-hybrid 2D volume matrix. From this point, the method is identical to the standard 2D MORASS[1] hybrid matrix methodology (Post et al., 1990) (or any other 2D NOESY complete relaxation matrix method can be used), where the hybridized 2D volume matrix is diagonalized to yield the complete relaxation matrix from which the inter-proton distances are calculated and used in restrained MD refinement. The output structure from the MD is then used as the new model structure in the next iteration. The entire procedure, including data simulation, is repeated until internal consistency among the calculated and observed 2D and 3D spectra and the output structures is reached. Figure 2 is a flow chart of the 3D hybrid-hybrid matrix method. It is worth noting that only a small fraction of the 3D data needs to be simulated, thus the method scales similarly to the relaxation matrix method, which scales only with the square of the number of spins.

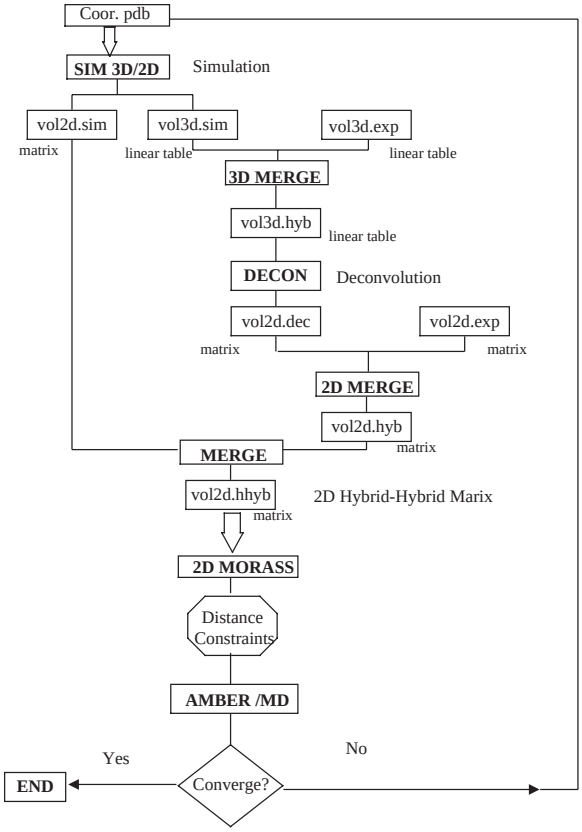

Figure 2. The hybrid-hybrid relaxation matrix refinement procedure. The initial structure is used to simulate NOE data for the first iteration. Experimental 3D data is scaled and merged with simulated 3D data to make a linear table of 3D volumes. Deconvoluted 2D data is merged with any available experimental 2D data. This hybrid matrix is then merged with simulated 2D data to form a complete 2D volume matrix. The structures resulting from the standard 2D MORASS refinement are used in subsequent iterations until convergence is reached.

Materials and methods

Sample preparation

All oligonucleotides used in this study were obtained from the Midland Certified Reagent Company (Midland, TX). All oligos were chemically synthesized on a 10 μmol scale using phosphoramidite chemistry and purified by reverse-phase and anion-exchange HPLC. Purity was assessed by HPLC and NMR. The purified oligonucleotides constituting each junction were dissolved individually in D_2O and quantitated by UV absorption using molar extinction co-efficients calculated according to nearest neighbor parameters (Puglisi and Tinoco, 1989). Stoichiometric samples of the three strands were assembled by NMR titration using the quantities calculated from UV absorption as a guideline. Titrations were performed at 80 °C in D_2O solvent by simultaneously monitoring the well-resolved methyl and aromatic regions of the spectrum. The sample was lyophilized and redissolved in phosphate buffer containing of mm sodium phosphate (pH 6.8), 0.5 mM EDTA, 10 mM $MgCl_2$ and 100 mM

[1]MORASS program can be downloaded from nmr.utmb.edu/#mrss.

NaCl. The sample was concentrated by ultra-filtration using a Centricon-3 centrifugal concentrator. The sample was lyophilized again and dissolved in 99.996% D_2O. The final concentration of the sample was about 2 mM.

NMR spectroscopy

3D NOESY-NOESY was collected at 28 °C at 750 MHz on a Varian UnityPlus instrument. The relaxation delay was set at 0.9 s and the acquisition time was 72 ms. The spectral sweep width was 7100 Hz in all three dimensions. The two mixing times were both 200 ms. This mixing time was selected to give optimal NOE transfer between spins in the NOE build-up phase. Residual water suppression was achieved by a low-power saturation pulse at the water frequency just prior to the first 90° pulse and during the two mixing periods. Homospoil pulses were applied during both mixing times to eliminate residual magnetization present within the *xy*-plane during the mixing times. No attempt was made to suppress zero-quantum interference during the mixing times. In the direct detection dimension 512 complex points were acquired, and for each of the two indirect dimensions 128 complex points were acquired. For each (t_1, t_2) pair, 8 scans were acquired. Quadrature detection in F1 and F2 was achieved using the hypercomplex method (States et al., 1982). To achieve a good S/N ratio and spectral dispersion, the experiment time was 228 h. This experiment time can be reduced considerably, however, without significantly compromising the quality of the data.

The 3D data set was processed using Felix software (version 95; Biosym, Inc., San Diego, CA). The data (128×128×512 points) was processed to give a data matrix of 256×256×1024 real data points after zero-filling in all three dimensions. Only the real part of the final spectrum was stored. A 90° shifted sine bell apodization function was used in all three dimensions. Baseline correction was done using the FLATT (Guntert and Wüthrich, 1992) routine available in Felix.

A 2D NOESY spectrum was collected at 28 °C at 750 MHz with an NOE mixing time of 200 ms. The NMR parameters for the 2D NOESY were: 3.5 s relaxation delay, spectral width 7100 Hz in both dimensions, 2K complex points in the direct detection dimension and 256 points in the indirect dimension. The 2D NOESY data was also processed by Felix.

Assignments of proton chemical shifts were based on previously reported values by Leontis et al. (1995). Most of the chemical shifts were found to be identical with the previously reported values, except for the two cytosines at the ends. The cross peaks were picked using the automatic peak-picking option available in the Felix program. The bounding box for each peak of interest was manually adjusted to reflect the actual linewidth of the peak.

Refinement methods

The 3D NOESY-NOESY volumes were deconvoluted into 2D NOESY volumes using the procedures described above (Zhang et al., 1995). Distance restraints, derived from the deconvoluted 2D peaks using MORASS, were used in structural refinement using AMBER (version 5.0; Case et al., 1997). Three different starting model coordinate sets were obtained based on a previously reported 2D NOESY structure (Ouporov and Leontis, 1995) determined using X-PLOR (Brünger, 1993). This structure was distorted by heating to 800 K; then three coordinate sets were randomly selected while the structure was cooled down slowly to 298 K. The rmsd between the three starting structures was 3.2 Å. Each of these starting structures was then refined separately using our iterative MORASS-3D hybrid-hybrid relaxation matrix method. For each refinement, the starting structure was placed in a periodic box of water containing a total of 1720 water molecules along with 29 counterions (one sodium counterion for each phosphate group) and was equilibrated for 10 ps using AMBER. This equilibrated structure was then used as the starting model for the next iteration. The errors (i.e. uncertainties) in the calculated proton-proton distances were described using a flat-well energy penalty function (Luxon and Gorenstein, 1995) in which the width of the flat-well is defined as a percentage of the equilibrium interproton distance, $\mathbf{r}_{ij}^{eq}$. For each of the starting structures the flat-well span was decreased from an initial value of ±25% $\mathbf{r}_{ij}^{eq}$ to ca. 10% while the distance restraint force constants were increased accordingly as the structures approached convergence.

To ensure Watson–Crick base-pairing in the helix, hydrogen bond restraints at an equilibrium distance of 1.9 Å were added between the base pairs in each arm of the 3WJ. The force constant on each hydrogen bond restraint was 15 kcal/mol·Å^2 with a flat-well distance error of ±12%. Only one hydrogen bond restraint was applied to either AT (between N1 of A and H3 of T) or GC base pairs (between H1 of G and N3 of C) to allow propeller twist between the base pairs during the refinement.

We have previously reported (Gorenstein, 1994) that large amplitude ϵ and ζ torsional angle fluctuations can occur during r-MD. Fluctuations for these two important torsional angles indicate transitions between low energy B_I conformations and higher energy B_{II} conformations. These results clearly demonstrated that there are significant variations in the relative populations of B_I and B_{II} conformations for duplex oligonucleotides in solution. Therefore, although our NOEs clearly establish B-DNA conformations for the 3WJ stems, no restraints were applied to the dihedral angles, thus allowing a greater degree of conformational flexibility. This eliminates artificial claims of higher precision in the refined structures.

During r-MD, the non-bonded interaction cutoff distance was set to 8 Å and a distance dependent dielectric constant was used with an integration time step of 1 fs. The charges at the 5′ and 3′ ends of the DNA strands were modified to avoid nonphysical electrostatic interactions.

For each iteration, a partial set of hybrid 3D volumes was obtained by scaling a set of experimentally determined 3D volumes by a set of corresponding simulated 3D volumes calculated from the starting model. Scaling between the simulated and experimental 3D volumes was performed using a linear regression over all experimental 3D volumes (see Equation 6 and Figure 2). These were in turn deconvoluted to generate a partial set of 2D volumes. 2D NOESY experimental volumes were then added to this partial set of deconvoluted 2D volumes (except when the identity of the experimental 2D cross peak was the same as the 2D deconvoluted cross peak) to form a new hybrid 2D volume matrix. This 2D hybrid volume matrix was then used as the 'experimental' 2D NOE input data for our standard MORASS/r-MD procedure in which the experimental volumes are merged with the full set of simulated volumes to generate a complete volume matrix. This hybrid-hybrid volume matrix is then diagonalized and the relaxation rate constants are calculated.

The 2D MORASS calculations used an isotropic tumbling model with a 3 ns correlation time to calculate interproton distances from the NOESY volumes. Previous calculations by others (Mujeeb et al., 1993) indicate that linear DNA molecules with less than 13 base pairs behave isotropically. Therefore, by simple center of mass arguments, the 3WJ DNA in this study should behave at least isotropically. Distance restraints calculated by MORASS from the relaxation rate matrix were then used with AMBER to generate a new structure that was more consistent with the NOE distance restraints.

For the r-MD procedure, the starting structure was first energy minimized against the NOE restraints for 3000 steps, followed by 8 ps of r-MD with temperature annealing (the temperature was increased from 298 K to 600 K in 2 ps; then cooled down to 298 K over the next 3 ps; continued at 298 K for the last 3 ps). Then, the average structure from the last 3 ps of r-MD was energy minimized, the resulting structure being used as the starting structure for the next iteration of MORASS.

The progress of the iterative refinement process to convergence was monitored by several key indicators. The rms error in the volumes was used as the first criterion for monitoring the refinements. The %rms(volume) is given by:

$$\%\text{rms (volume)} = \sqrt{1/N \sum_{ij} \left(\frac{v_{ij}^a - v_{ij}^b}{v_{ij}^a} \right)^2} \times 100\%, \tag{7}$$

where *a* or *b* can be either the experimental/deconvoluted or theoretical 2D volumes to give the %rms(exp) or %rms(the), respectively.

An R-factor, similar to the R-factor used in X-ray crystallography, was also used as a refinement criterion. The R factor is given by:

$$R = \frac{\sum_{ij} \left| v_{ij}^a - v_{ij}^b \right|}{\sum_{ij} v_{ij}^a} \tag{8}$$

For 2D matrix methods, we have suggested that the %rms(volume) is a very useful measure of quality of fit to the spectra since it weighs the percentage differences in the theoretical and experimental volumes for both large and small cross peaks equally. Thus, the %rms(volume) is more sensitive to weaker cross peaks which correspond to longer range (e.g. interresidue) distances. Similarly, the R-factor is regarded as a poorer measure of the quality of the refined structure since it is often dominated by the largest cross peaks. Another figure of merit for the quality of fit, the Q(1/6) factor (Thomas et al., 1991), also appears to better reflect the quality of the structure since it weighs

the weak cross peaks more heavily than the R-factor. The Q(1/6) factor is defined as

$$Q(1/6) = \frac{\sum_{ij} \tau_m \left| (v_{ij}^a)^{1/6} - v_{ij}^b)^{1/6} \right|}{\sum_{ij} (1/2)\tau_m \left| (v_{ij}^a)^{1/6} + v_{ij}^b)^{1/6} \right|} \quad (9)$$

All of these refinement factors are based upon 2D volumes. We have found that they parallel figures of merit defined by the experimental and theoretical fits to 3D volumes, thus either 2D or 3D figures of merit appear to be equally acceptable (Zhu et al., 1996).

Measurement of conformational flexibility of helical arms

The three final structures obtained by the iterative MORASS/r-MD procedure were averaged to a single structure using AMBER5:CARNAL (Ross, 1995). This structure was subsequently minimized with no restraints by first 1000 steps of steepest descent minimization, then another 1000 steps of full conjugate gradient minimization using AMBER5:SANDER. The minimized structure was then edited in AMBER5:XLEAP (Schafmeister et al., 1995) to add 29 Na^+ counterions to achieve charge neutrality. The counterions alone were then minimized for 2000 steps (as above) using the belly option. XLEAP was then again used to add 4512 triangulated 3-point (TIP3P) waters (Jorgensen and Tirado-Rives, 1988) to the 3WJ-counterion structure, resulting in a total number of 14572 atoms in the system. The TIP3P solvent was disordered in three steps. First, the solute atoms were held in fixed positions using 500 kcal/mol·Å^2 harmonic Cartesian restraints while the solvent (including the counterions) was minimized for 2000 steps. In the second water step, the solvent was subjected to 25.0 ps of unrestrained constant pressure MD with a 2.0 fs time step, SHAKE (Ryckaert et al., 1977; van Gunsteren and Berendsen, 1977) was applied to all bonds involving hydrogen, and periodic boundary conditions while the solute continued to be fixed with 500 kcal/mol·Å^2 harmonic Cartesian restraints. During this run the system temperature was ramped gradually from 100 K to 300 K over the first picosecond to avoid localized superheating. It is important to note that in this run and all subsequent runs using Cartesian restraints, the fixed atom coordinates used as anchoring points were the final atomic coordinates from the previous run. Thus, a small amount of compensatory solute movement is likely over a series of runs using harmonic Cartesian restraints. In the third and final water equilibration step, the Particle Mesh Ewald summation (PME) option (Darden et al., 1993; Essman et al., 1995) was toggled on with a B-spline interpolation order of 4 to rigorously conserve energies. As described in the AMBER5 manual, the PME method 'is a fast implementation of the Ewald summation method (Ewald, 1921) for calculating the full electrostatic energy of a periodic box in a macroscopic lattice of repeating images'. It has been shown to work especially well with nucleic acid systems (B. Luxon, unpublished; Cheatham, 1996). Box sizes were typically 68 × 58 × 48 Å during all PME MD runs. Thus, a further 25.0 ps of 300 K MD with a 2.0 fs time step and SHAKE was executed while continuing the 500 kcal/mol·Å^2 Cartesian restraints on the solute atom positions. At this point the harmonic Cartesian restraints on the solute were relaxed from 25.0 to 0.0 kcal/mol·Å^2 in seven steps. In step I the solute restraints were reduced to 25 kcal and the system was subjected to 1000 steps of steepest descent minimization using the PME option. In step II 3.0 ps of PME/MD at 300 K with SHAKE on all bonds to hydrogen was run using 25 kcal/mol·Å^2 Cartesian restraints on the solute. In steps III–VII the system was subjected in each step to 1000 steps of minimization with PME while the Cartesian restraints on the solute atom positions were reduced in steps of 5 kcal/mol·Å^2 so that in step VII there were no restraints whatsoever.

At this point equilibration of the system was begun by running 50.0 ps of unrestrained constant pressure PME/MD with a 2.0 fs time step, SHAKE was applied to all bonds involving hydrogen, 10.0 Å cutoff, and periodic boundary conditions while the temperature was ramped gradually from 100 K to 300 K over the first picosecond. A single harmonic imino H-bond restraint of 50 kcal/mol·Å^2 was placed between each of the last four base pairs of each duplex arm to reduce fraying and other end artifacts. After this run, a production phase of 250 ps of PME/MD was performed with the only exception being that 5 kcal/mol·Å^2 imino restraints were used on the ends instead of 50 kcal/mol·Å^2. Thus, a total of 3000 coordinates sets were accumulated in the full 300 ps of PME/MD trajectory during the equilibration and production phases. The 300 ps PME/MD equilibration and production runs were repeated four additional times using the following different combinations of NMR distance restraints: (a) 5 kcal/mol·Å^2 with a ±20% flatwell; (b) 25 kcal/mol·Å^2 with a ±25% flatwell, (c) 25 kcal/mol·Å^2 with a ±10% flatwell, and (d) 100 kcal/mol·Å^2 with a ±10% flatwell.

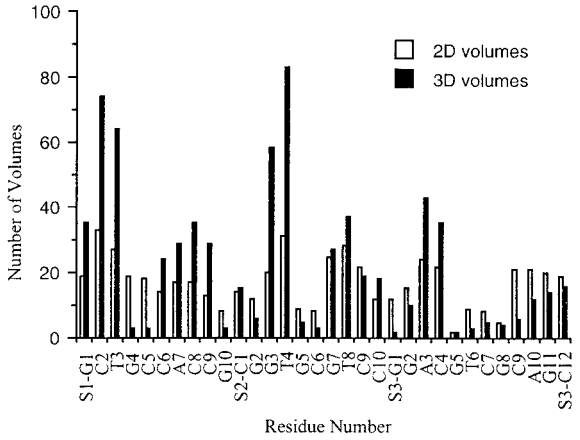

Figure 3. Number of NOE integrals obtained from 2D NOESY and 3D NOESY-NOESY experiments.

The five resulting trajectories were analyzed using AMBER5:CARNAL. In particular, the angles between each of the arms of the 3WJ were measured as a function of time in order to determine the influence of the NMR distance restraints on the relative movement of the three DNA helical arms. This was accomplished by first defining a 'fiducial reference' for each arm as being a line drawn through the center of mass (CM) of the first (i.e. end) base pair and the CM of the fourth base pair in. CARNAL was then instructed to measure as a function of time the angles between these reference lines for helices X-H, X-R, and H-R.

Results and discussion

Proton assignments

Assignments of proton chemical shifts were based on previously reported values by Leontis et al. (1995). Except for residues in the junction region, where NOE interactions are weak, the 3D NOESY-NOESY spectra gave higher numbers of measurable NOE peaks than the 2D NOESY spectra (Figure 3). A total of 6253 peaks were picked by the automatic peak-picking routine of Felix95. After removing the body diagonals, artifacts and noise peaks, 1635 peaks were retained. A total of 912 3D peaks (ijk and iji type peaks) were used for the deconvolution process. The remainder were cross-diagonals (iij type) peaks. The 2D NOESY experimental data set provided 78 volumes that were not obtained from the deconvolution of the 3D spectra. These 2D volumes (obtained directly from 2D NOESY experiment) were added to the deconvoluted 2D volumes set to form the hybrid-hybrid 2D volume matrix.

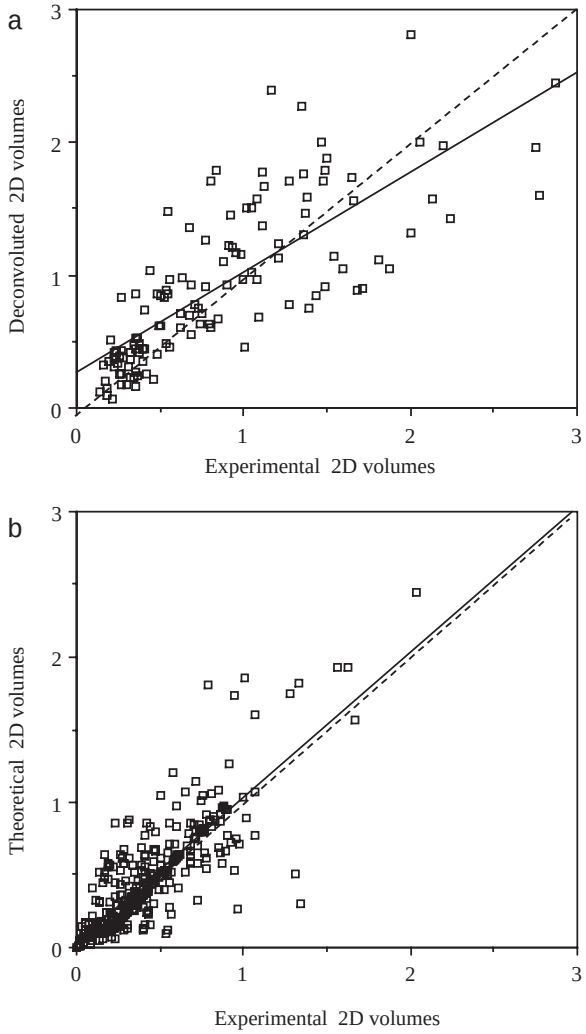

Figure 4. (a) Comparison of deconvoluted 2D volumes (obtained by deconvolution of 3D NOESY-NOESY volumes) against the experimentally determined 2D volumes. The solid line is the linear regression that yields a slope of 0.82. The dashed line shows the linear fit with a slope of unity. (b) Comparison of experimental 2D volumes versus theoretical 2D volumes. Theoretical volumes are calculated from the final structure. Experimental 2D volumes include deconvoluted 2D volumes (derived from experimental 3D NOESY-NOESY volumes) and experimental 2D volumes obtained from a 2D NOESY experiment. The linear regression (solid line) yields a slope of 0.99. The dashed line is the linear fit with a slope of unity.

Refinement convergence summary

The progress of the iterative refinement process was monitored by several key indicators summarized in Table 1. Both experimental and theoretical %rms (vol-

Table 1. Refinement example and summary of the quality of the refined structures for the DNA 3WJ

Iteration	Rms difference		R factor	$Q^{(1/6)}$ factor	E (const.) (kcal/mol/Å)	E(Tot) (kcal/mol/Å)
	%vol.(exp)	%vol.(the)				
1	127.9	226.4	0.451	0.109	21.25	−30054
2	111.3	192.4	0.447	0.101	30.38	−34187
3	91.9	158.2	0.440	0.098	43.13	−34417
4	80.3	142.1	0.402	0.091	92.04	−34435
5	78.2	121.4	0.391	0.085	97.62	−34477
6	75.2	115.0	0.374	0.079	149.45	−34403
7	75.8	72.7	0.375	0.071	190.12	−34393
8	76.4	73.1	0.371	0.067	213.29	−34329
Final[a]	80.3±4.5	72.1±10.8	0.341±0.002	0.061±0.002	232.3±31.6	−34376±49
Average[b]	79.0	68.6	0.343	0.063	238.4	−34359
2D	87.0	95.9	0.363	0.074	257.2	−34259

[a]Final represents the average (± standard deviation) of three different refinements using the 3D NOESY-NOESY data. Equivalent to the average of the individual 'simulated annealed' structures, <SA>.
[b]Average Structure $\overline{SA}$; averaged structure obtained by averaging the ensemble of 10 structures obtained during the 300 ps PME/MD.

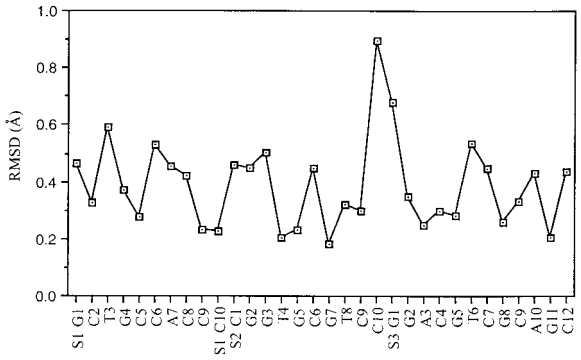

Figure 5. Rms deviation in Cartesian coordinates for each residue between the final 3WJ structures refined from 2D NOESY data and 3D NOESY-NOESY data.

ume) start at relatively higher numbers and gradually settle down to lower values with increased percentage of volume merging between the experimental and theoretical volumes. The MORASS procedure (Meadows et al., 1996) utilizes an incremental replacement of the theoretical volumes with the experimental values as the iterative refinement proceeds. This allows a more robust eigenvalue/eigenvector solution to the Bloch relaxation equations. The energy factors, such as the total energy, and the restraint energy also were monitored throughout the iterative process. Both the total energy and the restraint energy increased in value as the error bars and force constants on the restraints were tightened in the MD refinement. As expected, the R factor and the Q(1/6) factor were also found to decrease as the refinement progressed. The structures clearly improved at each refinement step (Table 1). For the refined structures, average deviations in bond lengths and bond angles from the ideal B-form geometry were calculated using the EDIT module of the AMBER program. These values are reported in Table 2.

Comparison of experimental 2D data to deconvoluted 2D data

Figure 4a shows the comparison of 2D volumes obtained by deconvolution from the 3D volumes, and the experimental 2D volumes. Random dispersion of data points shows there is no systematic error in the deconvolution process. The relaxation delay times were different for the 3D NOESY-NOESY (0.9 s) and the 2D NOESY (3 s) experiments, and that may explain the small deviation from unity slope (slope = 0.82) and linear regression fit which does not pass through the origin. Theoretical 2D volumes, calculated based on the final structure, are plotted against the experimentally determined 2D volumes (obtained by the deconvolution from 3D volumes). This is shown in Figure 4b. The rms deviation in Cartesian coordinates between the structures derived using only 2D NOESY data and 3D NOESY-NOESY data was calculated. The plot in Figure 5 shows the rms difference between these two structures for each base in the 3WJ molecule. Except for one base at the 3′ end of a helix, the rms differences agree quite well.

Table 2. Statistics of structural analysis for the final structures of the DNA 3WJ

Average deviations from ideal covalent geometry	<SA>[a]	$\overline{SA}$[b]
Bond length (Å)	0.013	0.011
Bond angle (°)	2.83	2.71
Rmsd between the three final structures[c]	0.9 Å (2.6 Å)	
Rmsd between the ensemble of 10 structures[c]	0.7 Å (2.3 Å)	

[a]For the three final structures derived from three independent refinements.
[b]For a single averaged structure obtained by averaging the ensemble of 10 structures obtained during the 300 ps PME/MD.
[c] For the rmsd calculations, the exterior terminal base pair of each helical stem was ignored. Numbers in parentheses are the rmsd values when the whole molecule is considered.

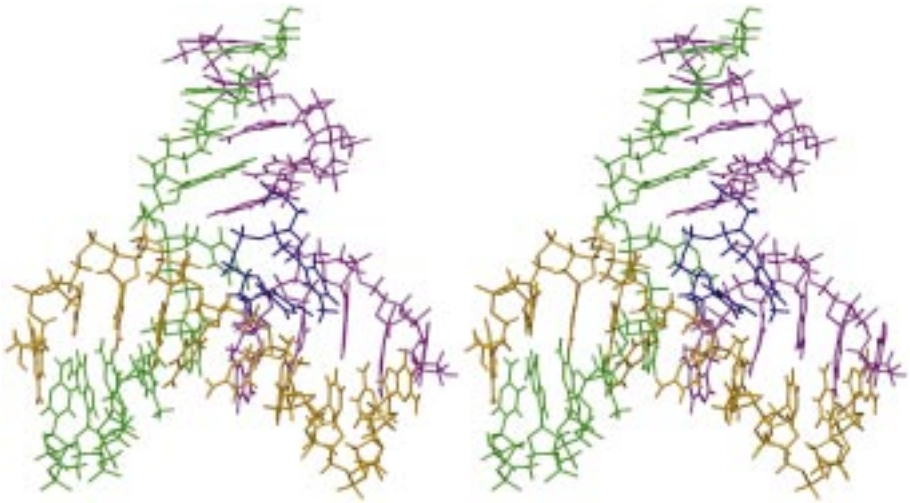

Figure 6. Stereoview of the final structure of the DNA 3WJ molecule. Only bonds between heavy atoms are shown. Strand x is in yellow, strand h in green, and strand r in magenta. The two unpaired bases are shown in blue.

Structure of the refined 3WJ

The RMSD among the three structures obtained from three independent refinements is 2.6 Å when all atoms are taken into account (Table 2). These three final structures were averaged to a single structure (shown in Figure 6). This averaged structure was then subjected to 300 ps of PME/MD as described previously. The purpose of the PME/MD calculations was to study the dynamics of the helical arms forming the 3WJ. A set of 10 final structures with lowest restraint energy obtained during the last 50 ps of the 300 ps MD trajectory are presented in Figure 7. The rmsd among these 10 structures is 2.3 Å when all the atoms are taken into account but only 0.7 Å when the base pairs at the exterior termini of each of the helical stems are ignored due to having a poor number of NMR restraints at the ends and dynamical fraying.

Gel electrophoresis studies have shown that there is a significant change in the conformation between 3WJs with and without unpaired bases in the junction region (Welch et al., 1993, 1995). 3WJs without any unpaired bases in the junction region form a flexible Y-shaped structure and remain in that conformation even in the presence of metal ions such as Mg^{2+}. Insertion of unpaired bases in the junction region allows the 3WJ molecule to form a more stable structure where co-axial stacking exists between two of the arms. Model building studies of DNA and RNA 3WJ lacking unpaired bases show that such structures can be built retaining all base pairs, but result in significant destacking at the junction due to conformational restraints (Leontis, unpublished observations). To maximize base stacking, one or more base pairs at the junction must therefore be disrupted. In addi-

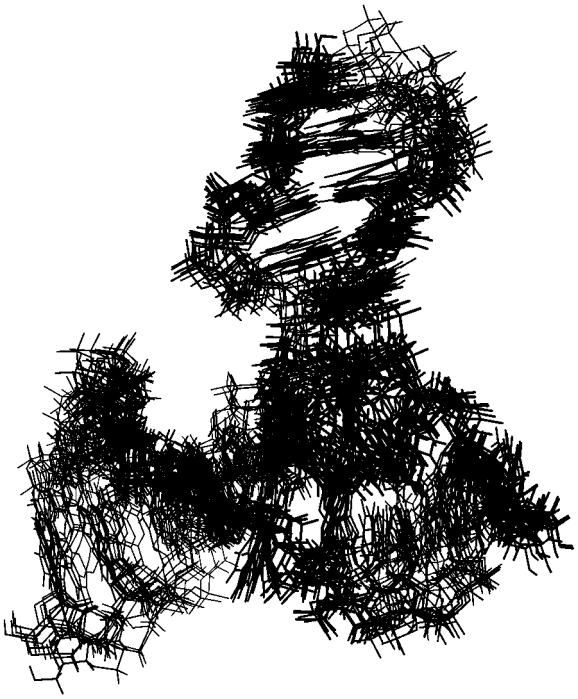

Figure 7. Overlay of 10 final structures with lowest restraint energy obtained during the last 50 ps of the 300 ps MD trajectory.

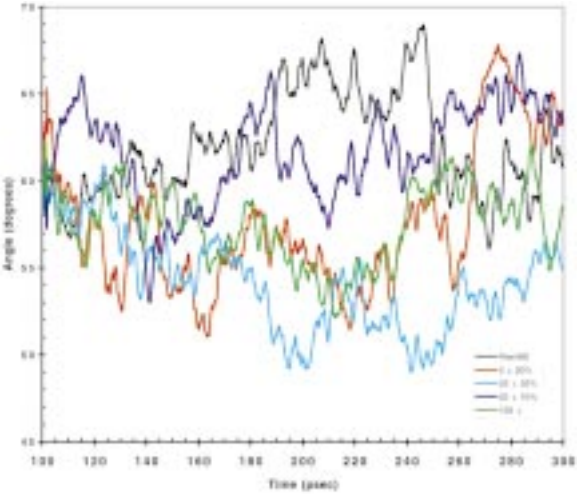

Figure 8. Inter-helical angle between the helical stems X and R as a function of time during the 300 ps MD. The other two inter-helical angles also showed fluctuations, irrespective of the energy and the error bars applied on the restraints. The five trajectories have different combinations of NMR distance restraints; Red: 5 kcal/mol·Å^2 with a +/−20% flatwell; Cyan: 25 kcal/mol·Å^2 with a +/−25% flatwell; Purple: 25 kcal/mol·Å^2 with a +/−10% flatwell; Green: 100 kcal/mol·Å^2 with a +/−10% flatwell; Black: free MD (no restraints).

tion, a model for an RNA 3WJ has been published in which there are no unpaired bases, but the structure involves several pseudo-knot structures, with the result that the junction is not bridged by three continuous strands (Felden et al., 1996). Recently reported crystal structures of hammerhead ribozymes (examples of RNA 3WJs) also show coaxial stacking between two of the helices (Pley et al., 1994; Scott et al., 1996). In the hammerhead ribozyme, a number of non-canonical purine-purine pairs form so that all the bases in the continuously stacked strand are paired.

Conformational flexibility and dynamics of helical arms

In the 3WJ structure reported here, the three helical arms of the 3WJ form two domains with coaxial stacking between helices X and H. The other helical domain (helix R), formed by the 5′ half of strand r and the 3′ half of strand x, stems out from the continually stacked domain. Both unpaired residues in the junction region are looped out (extra-helical) and are exposed to the solvent. The two bases stack upon each other and lie along the minor groove of helix X. Evidence for the coaxial stacking between helices X and H comes from inter-residue NOE cross peaks between residues x-C5 and x-C6. An imino-imino cross peak observed between h-G5 and r-G8 also provides additional evidence for coaxial stacking between these two helices. There is no evidence for a sequential NOE between the H1′ proton of h-G5 and the aromatic H6 proton h-C6. Evidence for the orientation of the third arm (helix-R), relative to the coaxially stacked stems, comes from the tertiary contact between the methyl group of the bulged r-T6 residue and the H4′ sugar proton of the r-G11 residue (Ouporov and Leontis, 1995).

Studies employing FRET experiments (Yang and Miller, 1996), gel-electrophoresis, and transient electric birefringence methods (Shen and Hagerman, 1994) showed that there is a greater degree of flexibility in the overall structure of the junctions with unpaired bases in the junction region. The FRET studies also showed that the bulged residues in the junction region introduce a point of flexibility into the structure of the 3WJ resulting in increased mobility of at least one of the helices flanking the bulge site. In the present study, the mobility of the helices was followed by measuring the angle between the helices over a 300 ps PME/MD equilibration (with or without restraints). Figure 8 shows the distribution of the angle between the stems X and R. The angle between helices X and R and the angle between helices H and R fluctuates to a greater extent than the angle between helices

X and H. As can be seen from the figure, irrespective of the force constant and the error bars applied on the restraints, the helices exhibit comparable mobility resulting in a change of the inter-helical angle ($\pm 20°$). Although the MD calculations are too short to investigate the full range of arm motion in the 3WJ, the trajectories provide direct support for the dynamic processes around the junction region.

Efficiency and precision of the hybrid-hybrid refinement method

In the hybrid-hybrid relaxation matrix method, a linear table is used for 3D volumes instead of a 3D matrix, since a 3D NOESY-NOESY volume matrix is a sparse matrix containing less than 1% non-zero elements. Using a linear table instead of a matrix virtually eliminates any significant increase in memory size, CPU time or storage space. Additional calculations for the 3D scaling, hybrid-hybrid matrix calculations and 3D NOESY-NOESY data deconvolution add little to the overall computational time.

Results from this structural refinement indicate that the hybrid-hybrid matrix methodology provides an efficient means to obtain distances from 3D NOESY-NOESY while taking into account multi-spin relaxation effects (spin diffusion). Both large molecular size and longer mixing times required for adequate S/N conspire to make spin-diffusion a greater problem in 3D versus 2D NOE spectra. The hybrid-hybrid relaxation matrix refinement method thus has particular utility in situations where 2D NOESY provides inadequate spectral resolution.

Further, as shown in Table 1, the various measures used to define the precision of the structure demonstrate that the 3D MORASS refined structure is of higher quality than the 2D refined structure. Various R-factors, the total energy as well as the restraint energy are lower for the 3D refined structure.

Conclusions

In this paper, a simple, efficient, and robust structure refinement method using 3D NOESY-NOESY data has been presented and successfully tested on experimental data obtained for the DNA 3WJ. This method uses a straightforward deconvolution scheme to obtain a hybrid-hybrid 2D NOESY volume matrix from 3D NOESY-NOESY volume data. The results clearly show that the hybrid-hybrid relaxation rate refinement approach is a promising method for solving structures of larger biomolecules that require three-dimensional NMR. Although sensitivity is still a problem, even at 750 MHz, this method has several obvious advantages.

This method does not rely on any experimental 2D data. It needs only 3D NOESY-NOESY experimental data and a reasonable starting model. Hence, this method is very suitable to study larger biomolecules for which significant numbers of good quality 2D NOESY cross peaks cannot be resolved. This method also provides a simple means to incorporate distance restraints derived from other heteronuclear experiments (e.g., 3D/4D heteronuclear filtered and edited NOESY experiments).

Acknowledgements

This work was supported by NIH (AI27744), NIEHS (ES06676), the Welch Foundation (H-1296) and the Sealy and Smith Foundation grants to D.G.G., and NSF CHE-9302619, NIH grants (R01-GM41454 and 1-R15-GM/OD55898-01), ACS-PRF (20871-GB4 and 31427-B4) to N.B.L. Building funds were provided by NIH (1CO6CA59098). The authors thank Mike Hills for helpful discussions.

References

Altona, C., Pikkemaat, J.A. and Overmars, F.J.J. (1996) *Curr. Opin. Struct. Biol.*, **6**, 305–316.

Anderson, R.J., Galatowicz, G., Macdonald, I.D., Lowdell, M.W., Corbett, T.J. and Prentice, H.C. (1997) *Exp. Hematology*, **25**, 256–262.

Belague, C., Kalla, M. and Zhang, W. (1997) *J. Virology*, **71**, 3299–3306.

Berg, J.N., Boelens, R., Vuister, G.W. and Kaptein, R. (1990) *J. Magn. Reson.*, **87**, 646–651.

Bernks, K.I. and Bohenzky, R.A. (1987) *Adv. Virus Res.*, **32**, 243–306.

Bernstein, R., Ross, A., Cieslar, C. and Holak, T.A. (1993) *J. Magn. Reson.*, **B101**, 185.

Birikh, K.R., Heaton, P.A. and Eckstein, F. (1997) *Eur. J. Biochem.*, **245**, 1–16.

Boelens, R., Vuister, G.W., Koning, T.M.G. and Kaptein, R. (1989a) *J. Am. Chem. Soc.*, **111**, 8525–8526.

Boelens, R., Koning, T.M.G., van der Marel, G.A., van Boom, J.H. and Kaptein, R. (1989b) *J. Magn. Reson.*, **82**, 290–308.

Bonvin, A.M.J.J., Boelens, R. and Kaptein, R. (1991) *J. Magn. Reson.*, **95**, 626–631.

Bothner-By, A.A. and Noggle, J.H. (1979) *J. Am. Chem. Soc.*, **101**, 5152–5155.

Brünger, A.T. (1993) *X-PLOR, version 3.1. A System for X-Ray Crystallography and NMR*, Yale University Press, London.

Case, D.A., Pearlman, J.W., Caldwell, T.E., Chetham III, T.E., Ross, W.S., Simmerling, C.L., Darden, T., Merz, K.M., Stanton, A.L., Cheng, J.J., Vincent, M., Crowley, M., Ferguson, D.M., Radmer,

R.J., Seibel, G.L., Singh, U.C., Weiner, P.K. and Kollman, P.A. (1997) AMBER 5, University of California, San Francisco, CA.
Cheatham III, T.E. (1996) *http://www.amber.ucsf.edu/amber/tutorial/polyA-polyT/*
Chastain, P.D. and Sinden, R.R. (1998) *J. Mol. Biol.*, **275**, 405–411.
Donne, D.G., Gozansky, E.K. and Gorenstein, D.G. (1995) *J. Magn. Reson.*, **106**, 156–163.
Duckett, D.R. and Lilley, D.M. (1990) *EMBO J.*, **9**, 1659–1664.
Essman, U., Perera, M.L., Berkowitz, M.L., Darden, T., Lee, H. and Pedersen, L. (1995) *J. Chem. Phys.*, **b103**, 8577–8593.
Ewald, P. (1921) *Ann. Phys.* (Leipzig), **64**, 253.
Felden, B., Florentz, C., Ciege, R. and Westhof, E. (1996) *RNA*, **2**, 201–212.
Gorenstein, D. (1994) *Chem. Rev.*, **94**, 1315–1338.
Guntert, P. and Wüthrich, K. (1992) *J. Magn. Reson.*, **96**, 403–407.
Guo, Q., Lu, M., Seeman, N.C. and Kallenbach, N.R. (1990) *Biochemistry*, **29**, 570–578.
Habazettl, J., Ross, A., Oschkinat, H. and Holak, T.A. (1992a) *J. Magn. Reson.*, **97**, 511–521.
Habazettl, J., Schleicher, M., Otlewski, J. and Holak, T.A. (1992b) *J. Mol. Biol.*, **228**, 156–169.
Jensch, F. and Kemper, B. (1986) *EMBO J.*, **5**, 181–189.
Keepers, J. and James, T.L. (1984) *J. Magn. Reson.*, **57**, 404–426.
Kessler, H., Seip, S. and Saulitis, J. (1991) *J. Biomol. NMR*, **1**, 83–92.
Ladbury, J.E., Sturtevant, J.M. and Leontis, N.B. (1994) *Biochemistry*, **33**, 6828–6833.
Lai, X., Chen, C. and Anderson, J. (1993) *J. Magn. Reson.*, **B101**, 271–288.
Leontis, N.B., Kwok, W. and Newman, J.S. (1991) *Nucleic Acids Res.*, **19**, 759–766.
Leontis, N.B., Hills, M.T., Piotto, M., Malhotra, A., Nussbaum, J. and Gorenstein, D.G. (1993) *J. Biomol. Struct. Dyn.*, **11**, 215–223.
Leontis, N.B., Hills, M.T., Piotto, M., Ouporov, I.V., Malhotra, A. and Gorenstein, D.G. (1995) *Biophys. J.*, **68**, 251–274.
Luxon, B.A. and Gorenstein, D.G. (1995) *Methods Enzymol.*, **261**, 45–73.
Ma, R.-I., Kallenbach, N.R., Sheardy, R.D., Petrillo, M.L. and Seeman, N.C. (1986) *Nucleic Acids Res.*, **14**, 9745–9753.
Macura, S. and Ernst, R.R. (1980) *Mol. Phys.*, **41**, 95–117.
Meadows, R., Post, C.B., Luxon, B.A. and Gorenstein, D.G. (1996) MORASS Program, University of Texas Medical Branch, Galveston, TX.
Mujeeb, A., Kerwin, S.M., Kenyon, G.L. and James, T.L. (1993) *Biochemistry*, **32**, 13419–13431.
Nussbaum, J.M., Newport, M.E.A., Mackie, M. and Leontis, N.B. (1994) *Photochem. Photobiol.*, **59**, 515–528.
Ouporov, I.V. and Leontis, N.B. (1995) *Biophys. J.*, **68**, 266–274.
Overmars, F.J.J., Pikkemaat, J.A., Van den Elst, H., Van Boom, J.H. and Altona, C. (1996) *J. Mol. Biol.*, **255**, 702–713.
Pley, H.W., Flaherty, K.M. and McKay, D.B. (1994) *Nature*, **372**, 111–113.
Post, C.B., Meadows, R.P. and Gorenstein, D.G. (1990) *J. Am. Chem. Soc.*, **112**, 6796–6803.
Puglisi, J.D. and Tinoco, I., Jr. (1989) *Methods Enzymol.*, **180**, 304–325.
Rosen, M.A. and Patel, D.J. (1993a) *Biochemistry*, **32**, 6563–6575.
Rosen, M.A. and Patel, D.J. (1993b) *Biochemistry*, **32**, 6576–6587.
Ross, W.S. (1995) CARNAL, University of California, San Francisco, CA.
Schafmeister, C.E.A.F., Ross, W.S. and Romanovski, V. (1995) LEaP (version 1.0) University of California, San Francisco, CA.
Shen, Z. and Hagerman, P.J. (1994) *J. Mol. Biol.*, **241**, 415–430.
Scott, W.G., Murray, J.B., Arnold, J.R.P., Stoddard, B.L. and Klug, A. (1996) *Science*, **274**, 2065–2069.
Shlyakhtenko, L.S., Rekesh, D., Lindsay, S.M., Kutyavin, I., Appella, E., Harrington, R.E. and Lyubchenko, Y.L. (1994) *J. Biomol. Struct. Dyn.*, **11**, 1175–1189.
States, D.J., Haberkorn, R.A. and Ruben, D.J. (1982) *J. Magn. Reson.*, **48**, 286–292.
Stuhmeier, F., Welch, J.B., Murchie, A.I.H., Lilley, D.M.J. and Clegg, R.M. (1997a) *Biochemistry*, **36**, 13530–13538.
Stuhmeier, F., Lilley, D.M.J. and Clegg, R.M. (1997b) *Biochemistry*, **36**, 13539–13551.
Thomas, P.D., Basus, V.J. and James, T.L. (1991) *Proc. Natl. Acad. Sci. USA*, **88**, 1237–1241.
Welch, J.B., Duckett, D.R. and Lilley, D.M.J. (1993) *Nucleic Acids Res.*, **21**, 4548–4555.
Welch, J.B., Walter, F. and Lilley, D.M.J. (1995) *J. Mol. Biol.*, **251**, 507–519.
Yang, M. and Miller, D.P. (1996) *Biochemistry*, **35**, 7959–7967.
Yip, P. and Case, D.A. (1989) *J. Magn. Reson.*, **83**, 643–648.
Yip, P. (1993) *J. Biomol. NMR*, **3**, 361–365.
Zhang, Q., Chen, J., Gozansky, E.K., Zhu, F., Jackson, P.L. and Gorenstein, D.G. (1995) *J. Magn. Reson.*, **B106**, 164–169.
Zhong, M., Rashes, M.S., Leontis, N.B. and Kallenbach, N.R. (1994) *Biochemistry*, **33**, 3660–3667.
Zhu, F.Q., Donne, D.G., Gozansky, E.K., Luxon, B.A. and Gorenstein, D.G. (1996) *Magn. Reson. Chem.*, **34**, 125–135.